Isotope and Phase Effects on the Proton Tautomerism in Polycrystalline Porphycene Revealed by NMR

ARTICLE *in* THE JOURNAL OF PHYSICAL CHEMISTRY A · MARCH 2009

Impact Factor: 2.69 · DOI: 10.1021/jp8079414 · Source: PubMed

THE JOURNAL OF PHYSICAL CHEMISTRY A

Article

Isotope and Phase Effects on the Proton Tautomerism in Polycrystalline Porphycene Revealed by NMR

Juan Miguel Lopez del Amo, Uwe Langer, Vero#nica Torres, Mariusz Pietrzak, Gerd Buntkowsky, Hans-Martin Vieth, Mohamed F. Shibl, Oliver Ku#hn, Martin Bröring, and Hans-Heinrich Limbach

J. Phys. Chem. A, **Article ASAP** • DOI: 10.1021/jp8079414

Isotope and Phase Effects on the Proton Tautomerism in Polycrystalline Porphycene Revealed by NMR†

Juan Miguel Lopez del Amo,‡ Uwe Langer,‡,# Verónica Torres,‡ Mariusz Pietrzak,‡,▽ Gerd Buntkowsky,§ Hans-Martin Vieth,|| Mohamed F. Shibl,‡,○ Oliver Kühn,‡,◆ Martin Bröring,⊥ and Hans-Heinrich Limbach‡,*

Institut für Chemie und Biochemie, Takustrasse 3, Freie Universität Berlin, D-14195 Berlin, Germany, Institut für Physikalische Chemie der Friedrich-Schiller Universität, Helmholtzweg 4, D-07743 Jena, Germany, Fachbereich Physik, Freie Universität Berlin, Arnimallee 14, D-14195 Berlin, Germany, Fachbereich Chemie, Philipps Universität Marburg, Hans-Meerwein-Strasse, 35032 Marburg, Germany

Received: September 7, 2008; Revised Manuscript Received: November 7, 2008

Using high resolution solid state ^{15}N and ^{2}H spectroscopy and longitudinal relaxometry we have studied the tautomerism of porphycene in the solid state, corresponding to a double proton transfer in two cooperative hydrogen bonds. The tautomerism is degenerate above 225 K but the degeneracy is lifted below this temperature, indicating a phase transition. Thus, the high-temperature phase is characterized by a dynamic proton disorder and the low-temperature phase by a dynamic proton order. ^{15}N magnetization transfer experiments obtained under cross polarization (CP) and magic angle spinning (MAS) conditions reveal the presence of two nonequivalent molecules A and B in the unit cell of phase II, exhibiting slightly different equilibrium constants of the tautomerism. Rate constants of the tautomerism in phase I could be obtained by the analysis of the longitudinal ^{15}N and ^{2}H relaxation times. The former, obtained at 9.12 MHz, exhibit a T_1 minimum around 270 K and are consistent with proton transfer induced dipolar $^{1}H-^{15}N$ relaxation mechanism. The latter, obtained at 46.03 MHz, exhibit a minimum around 330 K and arise from quadrupole relaxation. Within the margin of error, the rate constants of the HH and of the HD/DD tautomerism are the same, exhibiting a barrier of about 30 kJ mol^{-1}, as expected for an overbarrier reaction in a configuration with two compressed hydrogen bonds. By contrast, in the low-temperature phase a switch of the DD transfer kinetics into the nanosecond time scale is observed, exhibiting a non-Arrhenius temperature dependence which is typical for tunneling. This increase of the rate constants by lowering the temperature is discussed in terms of a switch from a concerted HH transfer in phase I to a stepwise transfer in phase II, where intermolecular interactions lower the energy of one of the cis-intermediates.

Introduction

Since its discovery, the tautomerism of porphycene (Figure 1)[1] has been a challenge for experimental and theoretical chemistry.[2−4] This molecule exhibits two short intramolecular N−H···N hydrogen bonds in the crystalline state as demonstrated by room-temperature X-ray crystallography.[5] The molecular packing is illustrated in Figure 2. The asymmetric unit consists of only half a molecule because the molecule is located on an inversion center. A second molecule in the unit cell is related to the first one by symmetry. These findings imply that the two imino hydrogens are dynamically disordered at room temperature. In a ^{15}N CPMAS NMR study of the polycrystalline material some of us indeed provided evidence that all nitrogen atoms are equivalent, i.e., that the protons in this compound are subject to a rapid degenerate tautomerism[1] confirming the room-temperature X-ray structure. In this regime, rate constants were measured by ^{15}N relaxometry,[6] revealing values of about 10^7 s^{-1} corresponding to a barrier of about 32 kJ mol^{-1}. However, below 225 K temperature, the spectra suddenly changed which could indicate a phase transition. Now, four signals were observed, shifting away from each other when temperature was lowered. This observation indicated the presence of four nonequivalent nitrogen atoms with temperature dependent proton densities below 225 K.[1] Such a situation could be interpreted in two different ways. Either a single type of molecule is present having access to all four tautomeric states 1 to 4 in Figure 1a, or two types of molecules A and B are present as illustrated in Figure 1b, where for each molecule only two tautomeric states 1 and 2 can be observed characterized by slightly different equilibrium constants. Thus, it could not be decided whether the reaction is stepwise as in the parent compound porphyrin[7] or whether it is concerted as illustrated in Figure 1.

The tautomerism of porphycene exhibits other intriguing aspects. Malsch and Hohlneicher[8] have performed a matrix isolation study of porphycene and measured IR, Raman, and UV/vis spectra, as well as site-selective fluorescence and fluorescence excitation spectra. In spite of many efforts, the NH-stretching vibrations could not be identified. Waluk et al.[9] have

† Part of the "Max Wolfsberg Festschrift".

* Corresponding author. E-Mail: limbach@chemie.fu-berlin.de.
‡ Institut für Chemie and Biochemie, Freie Universität Berlin.
§ Friedrich-Schiller Universität, Jena.
|| Fachbereich Physik, Freie Universität Berlin.
⊥ Philipps Universität Marburg.
Present address: Bruker Biospin, Rheinstetten-Forchheim, Germany.
▽ Present address: Institute of Physical Chemistry, Polish Academy of Sciences, Kasprzaka 44/52, 01-224 Warsaw, Poland.
○ Present address: Department of Chemistry, Faculty of Science, Cairo University, Cairo, Egypt.
◆ Present address: Institut für Physik, Universität Rostock, Universitätsplatz 3, D-18051 Rostock, Germany.

10.1021/jp8079414 CCC: $40.75

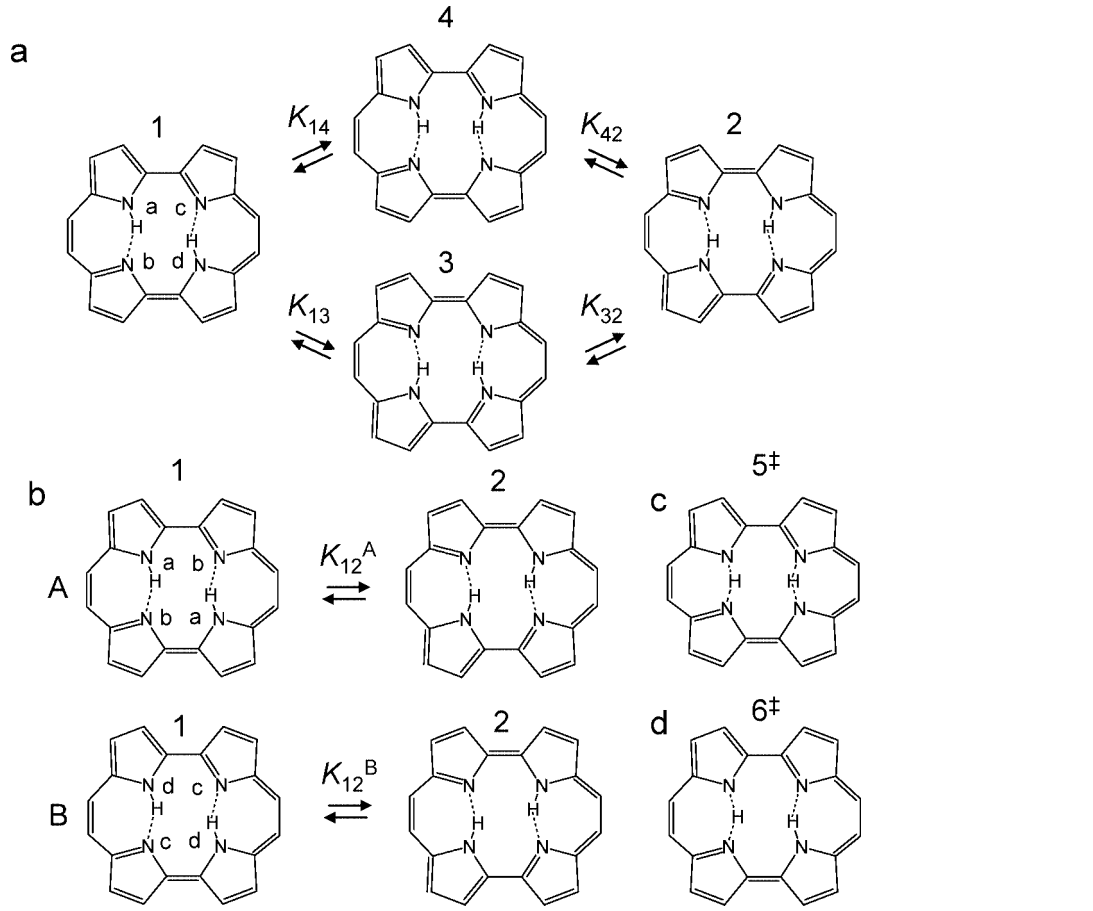

Figure 1. Stepwise vs concerted tautomerism of porphycene in the crystalline state according to ref 1. (a) Exchange model involving single proton transfers between spectroscopically observable trans and cis tautomeric states 1 to 4. (b) Exchange model involving two nondegenerate double proton transfers between trans tautomers 1 and 2 in two different molecules A and B in the asymmetric unit, characterized each by slightly different equilibrium constants K_{12}^{A} and K_{12}^{B}. (c) Transition state $5^{\ddagger}$ of a concerted double proton transfer between states 1 and 2. (d) Transition state $6^{\ddagger}$ of single proton transfer between state 1 and intermediate state 3.

observed tunnel splittings in the UV spectra of electronically excited porphycene in the gas phase, indicating a coherent concerted double proton tunneling process in the ground and the electronic excited state. On the other hand, a rate process has been observed in the first excited-state of porphycene embedded in a polymer matrix which was attributed to a double proton transfer,[10] exhibiting a very small activation energy of about 2 kJ mol^{-1}. This process was attributed to the mode-specific activation of a low-frequency vibration of the skeleton which promotes the hydrogen transfer. Some of us have recently analyzed H/D isotope effects on the chemical shifts of the hydrogen bond protons which revealed H/D isotope effects on the hydrogen bond geometries[11] which were analyzed theoretically.[12] It was shown that the two hydrogen bonds exhibit a vicinal coupling in the sense that compression of the first bond leads also to the compression of the second. Thus, the concerted pathway was suggested to dominate, implying a two-stage process, i.e. concerted hydrogen bond compression followed by a more or less concerted double proton transfer.

Quantum-chemical studies indicated a borderline case in porphycene between a stepwise and a concerted double proton transfer. More recent calculations predict the trans-form to be more stable than the cis-form, as well as a stepwise pathway which is in terms of the barrier slightly favored over the concerted pathway.[13−15] Barriers of about 20 kJ mol^{-1} were calculated for the stepwise and of about 26 kJ mol^{-1} for the concerted pathway, where zero-point energy contributions were not taken into account. Inclusion of zero-point energy in

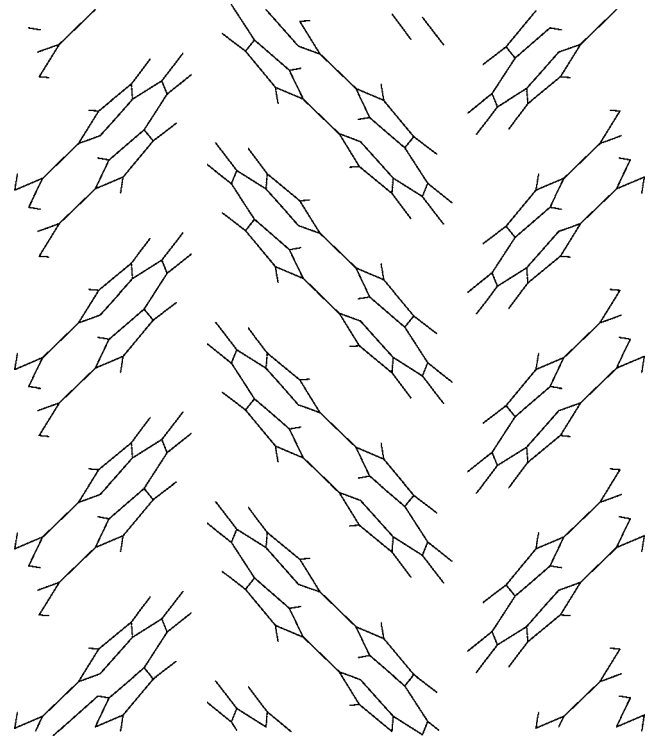

Figure 2. Crystal structure of porphycene according to ref 5. Adapted from ref 1.

the harmonic approximation, however, results in a barrier which is lower for the concerted pathway.[13]

Recently, Smedarchina et al.[16] have explored theoretically the kinetic HH/HD/DD isotope effects on the concerted and the stepwise transfer. It was noted that there is a discrepancy between the observed tunneling splitting[9] and the observed rate constants:[6] the former would require a lower and the latter a higher barrier of tautomerism. Thus, the lack of experimental data did not allow drawing a final conclusion on the mechanism.

These results indicate that the tautomerism of porphycene depends very much on the environment, in contrast to the isomer porphyrin.[7] In particular, the question arises whether the environment can lead to a switch from a concerted to a stepwise reaction mechanism. Such a mechanism has been proposed recently for the photoinduced double proton transfer in azaindole dimers.[17]

In view of the general importance of environment dependent proton transfer in nature[18] the goal of the present work was, therefore, to study further the effects of isotopic substitution as well as the effect of the solid environment on the tautomerism of porphycene. As shown previously in a number of different cases, for this purpose, a combination of solid state ^{15}N and ^{2}H solid state NMR and NMR relaxometry is well suited.[19−21] We note that ^{1}H and ^{2}H relaxometry have been shown to be powerful tools for the study of proton and deuteron transfer in hydrogen bonded solids,[22−24] in particular benzoic acid dimers.[25]

This paper is organized as follows. After the Experimental Section, the results of our measurements are described and discussed.

Experimental Section

The synthesis of ^{15}N enriched porphycene has been described previously.[1,5] Deuteration of the inner mobile proton sites was first done by refluxing for 1 h in pure CH_3COOD. The solid deuterated samples were closed with a plastic cap and stored between measurements in an desiccator over a small amount of liquid D_2O in order to prevent reprotonation by moisture, a process which we had observed for the structural isomer porphyrin.[7a]

The liquid state ^{1}H and ^{15}N NMR spectra of porphycene were measured using a Bruker AMX 500 spectrometer (500.13 MHz for ^{1}H, 50.68 MHz for ^{15}N). In order to reference the ^{15}N chemical shifts to external solid $^{15}NH_4Cl$ the relation $\delta(CH_3{}^{15}NO_2, \text{liquid}) = \delta(^{15}NH_4Cl, \text{solid}) - 341.168$ ppm was used.[26]

The ^{1}H decoupled ^{15}N CPMAS spectra were recorded at 9.12 and 30.12 MHz using Bruker CXP 100 and MSL 300 NMR spectrometers equipped with standard 5 mm and 7 mm Doty and Chemagnetics probes. We used a normal cross polarization sequence, which minimizes ringing artifacts,[27] with 3 to 8 ms cross polarization times, 6−10 μs ^{1}H-90° pulse width, 3 to 10 s recycle delay. For the measurement of the ^{15}N longitudinal relaxation times T_1 in connection with the CP scheme, a pulse sequence described by Torchia[28] was employed. Due to phase cycling of the first proton 90° pulse and of the receiver phase, the equilibrium magnetization is zero in this experiment, which is contrary to the most frequently applied inversion−recovery pulse sequence where equilibrium magnetization approaches maximum intensity. Between 500 and 2500 scans were accumulated on average, with a contact time for cross polarization between 1.5 and 5.0 ms, and a repetition time of 1 to 3 s. Low temperature measurements were carried out by passing nitrogen gas through a home-built heat exchanger[29] immersed in liquid nitrogen, thus allowing temperatures as low as 90 K to be achieved, maintaining the spinning speeds between 2 and 2.5 kHz which were large enough for obtaining essentially rotational sideband-free spectra. Chemical shifts were referenced to external solid $^{15}NH_4Cl$.

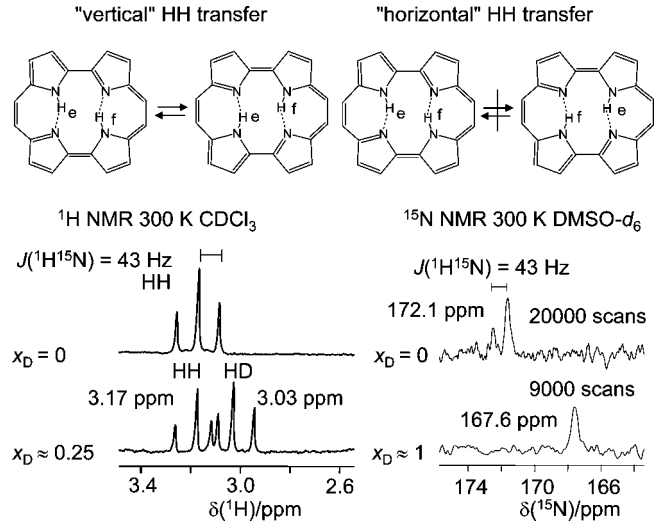

Figure 3. ^{1}H and ^{15}N NMR spectra of 95% ^{15}N enriched porphycene at 500.13 and 50.68 MHz at different deuterium fractions x_D. For further explanation, see text.

The measurements of the ^{2}H T_1 relaxation times of the deuterated samples were performed on a home-built 7 T spectrometer operating at a Larmor frequency of 46.03 MHz, equipped with a home-built low temperature ^{2}H probe. The measurements were carried out employing a saturation recovery pulse sequence followed by a solid echo sequence and recording of the echo. The saturation part involved a string of 90° pulses (4 μs) with nonequal spacing to avoid any undesired echo formations. The two 90° pulses of the solid echo sequence were spaced by 30 μs. Finally, the echo was Fourier transformed, allowing the evaluation of T_1 of individual lines in the spectrum.

Results

In this section, we first describe the results of our liquid and solid state ^{15}N and ^{2}H experiments from which information about the structure of porphycene and the thermodynamics of the solid state proton tautomerism is obtained. Information about the proton transfer kinetics is obtained in a second stage where the longitudinal relaxation times measured are analyzed.

Liquid State ^{1}H and ^{15}N NMR of Porphycene. In a first step, we measured some liquid state ^{1}H and ^{15}N NMR spectra of ^{15}N labeled porphycene at different deuterium fractions x_D in the mobile proton sites. The result are depicted in Figure 3. The inner proton signals at $x_D = 0$ give rise to a triplet characterized by a coupling constant of 43 Hz, arising from a fast intramolecular proton transfer between two nitrogen atoms, corresponding to the "vertical" HH transfer in the two strong hydrogen bonds of the two seven-membered ring chelate moieties.[30] No signs of a "horizontal" HH transfer are observed. Such a process would convert the triplet into a pentet as observed previously for meso-tetraphenylchlorin.[31] The ^{15}N NMR spectrum of porphycene in DMSO-d_6 exhibits an asymmetric doublet at 172.1 ppm. The asymmetry arises from an interference between the dipolar $^{1}H-^{15}N$ coupling and the ^{15}N chemical shift anisotropy in combination with the higher viscosity of the solvent as compared to $CDCl_3$.

After partial H/D substitution the remaining proton signal of the HD isotopolog is shifted upfield. This effect has been

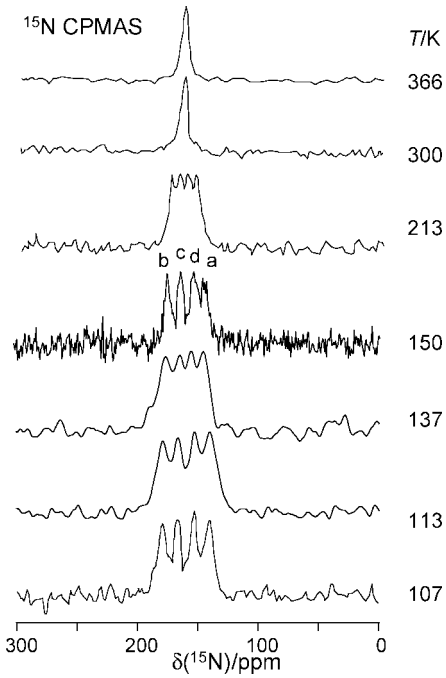

Figure 4. ^{15}N CPMAS NMR spectra of 95% ^{15}N enriched polycrystalline porphycene at 9.12 MHz as a function of temperature: 6 ms CP-time, 5 kHz spectral width, 2.7 s repetition time. Reference: external $^{15}NH_4Cl$. Adapted from ref 1. The spectrum at 150 K was acquired at 30.41 MHz.

TABLE 1: ^{15}N Chemical Shift Differences of Polycrystalline Porphycene

T/K	δ_{ba}/ppm	δ_{cd}/ppm
107	37.81	13.93
164	27.86	9.95
213	19.9	5.97
≥228	0	0

observed and discussed recently.[11,12] Deuteration of the first bond increases somewhat the N...N distance of this bond, and the distance of D to the H-bond center is slightly increased. This widening of the NDN bond also leads to a partial widening of the neighboring NHN-hydrogen bond which explains the high-field shift of the remaining proton. Along this line, we also observe now a related high-field ^{15}N signal shift in the doubly deuterated compound as illustrated in Figure 3. This is because the ^{15}N chemical shielding increases when the N....H distance is decreased.

As a conclusion, we will not consider in the analysis of the following results the "horizontal" process any longer, but only the "vertical" process.

Thermodynamics of the Solid State Tautomerism of Porphycene: Order−Disorder Phase Transition. *^{15}N CPMAS NMR Spectroscopy.* In Figure 4 are assembled the ^{15}N CPMAS NMR spectra of porphycene measured at 9.12 MHz which have been described previously.[1,6] The spectrum at 150 K was measured at 30.41 MHz in this study. Down to a temperature of about 225 K a single line is observed at 161 ppm with respect to solid $^{15}NH_4Cl$ which indicates that all four nitrogen atoms are equivalent, due to the presence of degenerate fast proton transfers. One may call this situation a "dynamic proton disorder". However, below 225 K the signal splits into four sharp lines, a−d, characterized by the chemical shifts δ_a, δ_b, δ_c, and δ_d. We assign this finding to a second order phase transition. It consists of a change from dynamic proton disorder above 225 K (phase I) to dynamic order below 225 K (phase II).

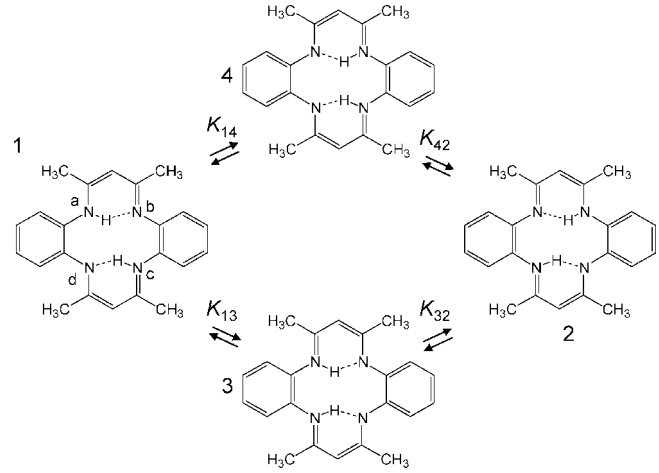

Figure 5. Solid state tautomerism of tetramethyldibenzotetraaza[14]-annulene (TTAA) according to refs 20, 31, and 32.

The splittings $\delta_{ba} = \delta_b - \delta_a$ and $\delta_{cd} = \delta_c - \delta_d$ in phase II increase slightly with decreasing temperature and are listed in Table 1. These observations have been explained[1,6] by the presence of two nonequivalent, asymmetric proton transfer systems

$$N_m{-}H\cdots N_n \rightleftarrows N_m\cdots H{-}N_n, \quad mn = ab, dc \quad (1)$$

in which the protons move very fast in slightly asymmetric double minimum potentials. One may call this phenomenon also "dynamic order". The two proton transfer systems are characterized by different proton density ratios given by

$$K_{ab} = (1 - \delta_{ba}/\Delta)/(1 + \delta_{ba}/\Delta), \quad K_{dc} = (1 - \delta_{cd}/\Delta)/(1 + \delta_{cd}/\Delta) \quad (2)$$

$\Delta = \Delta_N - \Delta_{NH}$ represents the intrinsic chemical shift difference between a protonated and a nonprotonated nitrogen atom. We assume that Δ is independent of temperature. Equation 2 can be rewritten as

$$\delta_{ba} = \Delta(1 - K_{ab})/(1 + K_{ab}), \quad \delta_{cd} = \Delta(1 - K_{dc})/(1 + K_{dc}) \quad (3)$$

As pointed out above and previously,[1,6] either each porphycene molecule contains all four types of nitrogen atoms, or there are two slightly different molecules A and B, where the first one contains atoms a and b, and the second atoms c and d. In the first case, the observation of the four lines indicates the presence of observable amounts of both trans- and cis-tautomers, whereas in the second case, for each molecule only two trans states are observed according to Figure 1, where cis-states could, however, be intermediate states of higher energy.

^{15}N CPMAS NMR Magnetization Transfer Experiments on Porphycene and Tetramethyldibenzotetraaza[14]annulene. In order to solve this problem, we performed in this study magnetization transfer experiments on porphycene at low temperatures. This transfer arises from ^{1}H induced spectral spin diffusion between ^{15}N atoms exhibiting small dipolar couplings if they are located within the same molecule.[32] However, such experiments are difficult to perform at low temperatures. Therefore, we tested the experimental setup using the well studied polycrystalline tetramethyldibenzotetraaza[14]annulene (TTAA) which exhibits a tautomerism according to Figure 5 as demonstrated by variable temperature ^{15}N CPMAS NMR.[20,33,34] As for porphycene in phase II, the ^{15}N CPMAS NMR spectra of TTAA also contain four lines a to d exhibiting temperature

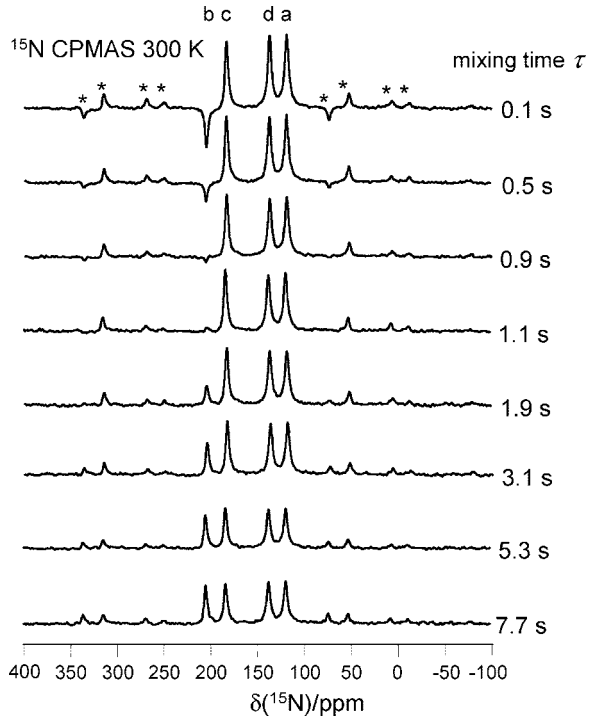

Figure 6. ^{15}N magnetization transfer experiment performed on polycrystalline tetramethyldibenzotetraaza[14]annulene-$^{15}N_4$ at 300 K and 30.41 MHz (7 T). For further information, see text.

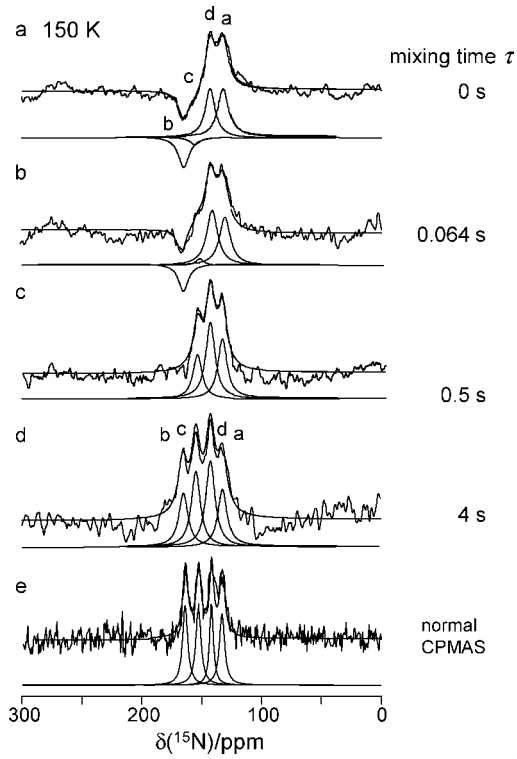

Figure 7. Superimposed experimental and calculated spectra obtained in a ^{15}N magnetization transfer experiment performed on polycrystalline porphycene-$^{15}N_4$ at 150 K and 30.41 MHz (7 T). For further information, see text.

dependent line separations which have been exploited as a chemical shift thermometer.[35] One- and two- dimensional magnetization transfer experiments indicated that each molecule contains all four nitrogen atoms a to d arising from a reduction of the molecular symmetry in the solid state and from the circumstance that the pairwise degeneracy of the tautomers is lifted by solid state interactions.

In these magnetization transfer experiments, a selective inversion of one or two lines could be achieved by introducing appropriate dephasing delays into the pulse sequences, a method which requires, however, well separated lines. Therefore, we used here a DANTE pulse sequence[36] incorporated into a CPMAS sequence where one NMR line is inverted or saturated via application of selective 180° pulses following the usual cross polarization sequence.[37]

The spectrometer settings for this experiment were first optimized at room temperature using TTAA as depicted in Figure 6. In the beginning of the mixing period, only line b is partially inverted. During the mixing period the negative magnetization is gradually transferred to the other lines to a similar extent, whose intensities, therefore, decrease at the same time. The magnetization transfer is complete after about 5 s before longitudinal relaxation becomes efficient. Thus, it follows that each molecule contains all four types of nitrogen atoms a to d as they are connected by spectral spin diffusion in view of the fact that the nitrogen atoms of TTAA are arranged approximately in a square with a side length of about 2.7 Å.[38]

In the next step we performed a similar experiment on phase II of porphycene at 150 K whose results are depicted in Figure 7. This experiment was much more difficult because of the low temperature and because of the much smaller line splittings as compared to TTAA. Thus, we were not able to invert only line b but also the magnetization of line c became slightly negative as illustrated by the line shape analysis in Figure 7a. We note that lines a and d exhibit similar intensities. The sum of all calculated lines is superimposed to the experimental spectrum. During the mixing period we observe that line a decreases more than line d, which indicates that the negative magnetization of line b is transferred only to line a but not to line d. After 4 s the intensities of lines a and b as well as those of lines c and d have equilibrated, but no equilibration is established between the two types of line pairs. This result is very different from the results found for TTAA in Figure 6. We, therefore, conclude that in contrast to TTAA, lines a and b of solid porphycene in phase II correspond to nitrogen atoms in molecule of type A, and line c and d to nitrogen atoms in another molecule of type B as was illustrated in Figure 1b. In other words, this means that each molecule contributes only two lines, or that in each molecule diagonally arranged nitrogen atoms are chemically equivalent.

Thermodynamics of the Tautomerism of Solid Porphycene. As the line splittings of the two line pairs of molecules A and B are different, it follows that they are characterized by different equilibrium constants of tautomerism between the two observable states 1 and 2 whose dependence on temperature can then be expressed as

$$K_{ab} = K_{12}{}^{A} = \frac{k_{12}{}^{A}}{k_{21}{}^{A}} = \frac{x_2{}^{A}}{x_1{}^{A}} = a_{12}{}^{A} \exp\left(-\frac{b_{12}{}^{A}}{T}\right),$$

$$a_{12}^{A} = \exp\left(\frac{\Delta S_{12}{}^{A}}{R}\right), \quad b_{12}{}^{A} = \frac{\Delta H_{12}{}^{A}}{R}. \quad (4)$$

$$K_{dc} = K_{12}{}^{B} = \frac{k_{12}{}^{B}}{k_{21}{}^{B}} = \frac{x_2{}^{B}}{x_1{}^{B}} = a_{12}{}^{B} \exp\left(-\frac{b_{12}{}^{B}}{T}\right),$$

$$a_{12}{}^{B} = \exp\left(\frac{\Delta S_{12}{}^{B}}{R}\right), \quad b_{12}{}^{B} = \frac{\Delta H_{12}{}^{B}}{R}. \quad (5)$$

$\Delta S_{12}{}^{A}$, $\Delta S_{12}{}^{B}$, $\Delta H_{12}{}^{A}$ and $\Delta H_{12}{}^{B}$ represent the reaction entropies and enthalpies for both molecules, R the gas constant and T the

absolute temperature, k_{12}^{A} and k_{12}^{B} the forward rate constants of the tautomerism. The degeneracy between the two states is lifted by the crystal lattice where the perturbation is slightly larger for molecule A than for molecule B.

By combination of eqs 2 to 5 the line splittings δ_{ba} and δ_{cd} can be expressed as a function of the inverse temperature. The spectral and thermodynamic parameters can then be obtained as described previously[6] by least-squares fitting to the experimental data as illustrated in Figure 8. The intrinsic line splitting Δ requires an additional comment. In our previous study[6] we had used a value of $\Delta = 46$ ppm; however, at that time we had not yet recognized the phase transition and had included the high temperature data into the fitting. Now, we obtain a better fit using a slightly smaller value of $\Delta = 42$ ppm by including only the data of the low-temperature phase II. We further note that Δ is substantially smaller than for the structural isomer porphyrin (108 ppm)[7] because hydrogen bonding is very weak in this molecule.[11]

The data of Figure 8 clearly exhibit a different behavior above and below 225 K. Above this temperature, the difference between both molecules A and B is absent, and both are characterized by an equilibrium constant of $K_{12} = 1$. However, below this temperature, suddenly the degeneracy is lost and both molecules A and B exhibit different temperature dependent equilibrium constants of tautomerism between forms 1 and 2. This confirms a phase transition around 225 K, which will be confirmed later by ^{2}H relaxometry.

All parameters obtained are assembled in Table 2. They allowed us to calculate the solid van't Hoff curves in Figure 8b. The reaction entropies are very small and the reaction enthalpies smaller than in solid tetraaza[14]annulenes.[31,33]

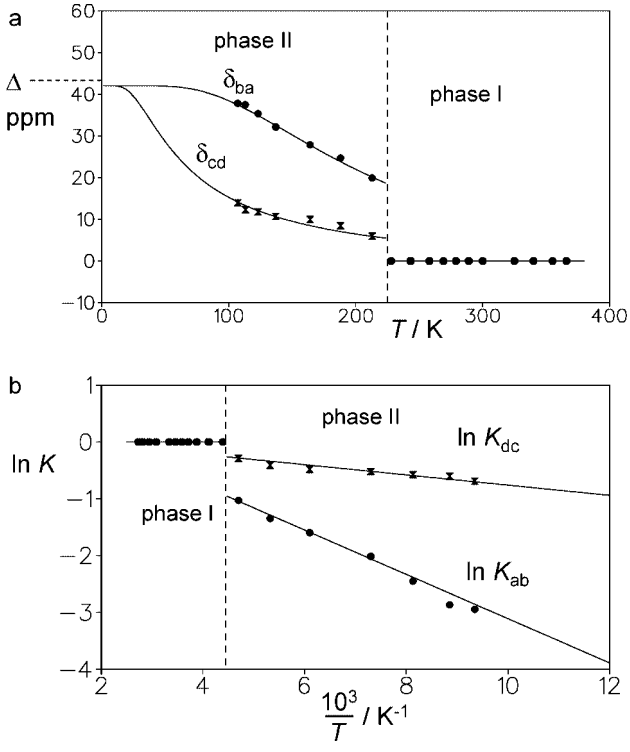

Figure 8. Thermodynamics of the porphycene tautomerism according to the exchange model of Figure 1b. (a) Comparison of the experimental temperature dependent chemical shift separations δ_{ba} and δ_{cd} defined in eq 2 with the theoretical values calculated as described in the text. Δ is the intrinsic chemical shift difference between nonprotonated and protonated porphycene nitrogen atoms. An order−disorder phase transition is observed around 225 K. (b) Van't Hoff diagram of ln K_{12}^{A} and ln K_{12}^{B} as a function of the inverse temperature.

TABLE 2: Parameters of the van't Hoff Analysis of Figure 8[a]

Δ	a_{12}^{A}	b_{12}^{A}	a_{12}^{B}	b_{12}^{B}	ΔS_{12}^{A}	ΔH_{12}^{A}	ΔS_{12}^{B}	ΔH_{12}^{B}
42	2.2	350	1.2	85	6.6	2.9	1.5	0.71

[a] Intrinsic chemical shift difference Δ in ppm, reaction enthalpies ΔH_{ij} in kJ mol^{-1} and reaction entropies ΔS_{ij} in J K^{-1}mol^{-1}.

TABLE 3: ^{15}N T_1-Relaxation Times and Rate Constants of the HH Transfer of Polycrystalline Porphycene According to Reference 6 Obtained under MAS Conditions at 9.12 MHz (2.1 T)[a]

T/K	T_1/s	k_{12}^{HH}/s^{-1}
228	3.4	4.2×10^6
243	1.43	1.1×10^7
243.5	1.5	1.1×10^7
258	1.04	2.0×10^7
269	0.97	2.7×10^7
279	0.98	3.6×10^7
289	0.99	3.8×10^7
300	1.07	4.9×10^7
325	1.28	7.2×10^7
340	1.62	1.1×10^8
355	2.7	3.7×10^8

[a] For further description, see text.

^{15}N longitudinal relaxation time measurements. In order to obtain information about the kinetics of the tautomerism longitudinal ^{15}N relaxation times had been measured previously[6] at 9.12 MHz (2.1 T) as a function of temperature. Exponential magnetization decays were observed in the whole temperature range. A ^{15}N T_1 minimum was observed around 270 K. The data are included in Table 3 and will be discussed later.

^{2}H NMR Spectroscopy. In order to confirm the observed phase transition and in order to prepare for ^{2}H longitudinal relaxation time measurements we have measured and analyzed the solid state ^{2}H spectra of static samples of porphycene deuterated in the mobile proton sites. We noted that the deuterium fraction decreased slightly with time when the solid was exposed to air, as found previously for the structural isomer porphyrin[7a] and in meso-tetraphenylporphyrin.[7c] This deuterium loss was manifested in losses of the ^{2}H signal intensities. On the other hand, the sample could be redeuterated by gaseous D_2O as present in an desiccator containing some liquid D_2O. Therefore, between measurements, porphycene was kept under such an atmosphere. Thus, we assign the results of all measurements to porphycene-d_2 rather than to porphycene-*hd*. However, we can not completely exclude a contribution of the latter to the relaxation times and hence to the rate constants obtained.

Some typical ^{2}H spectra of porphycene-d_2 are depicted in Figure 9. In phase I above 225 K a typical ^{2}H peak signal characterized by a quadrupole coupling constant of $q_{zz} = 143$ kHz and an asymmetry factor $\eta = 0$ is observed. A broad inner component indicates the presence of some deuterons in mobile species, probably arising from deuterated water or deuterated acetic acid used in the deuteration process. Their line shape contribution was neglected in the following analysis.

Below 225 K, temperature dependent line shapes were observed for phase II consisting of two components for molecules A and B, each affected by a fast deuteron tautomerism according to Figure 1. We used the program "NMR WebLab 4.1.2" of Spiess et al.[39] for the calculation of the deuteron line shapes of powdered samples in the presence of nondegenerate deuteron exchange between two sites. The simulations were performed using a natural line width of $W_o = 1/\pi T_2 = 1/0.05\pi$Hz

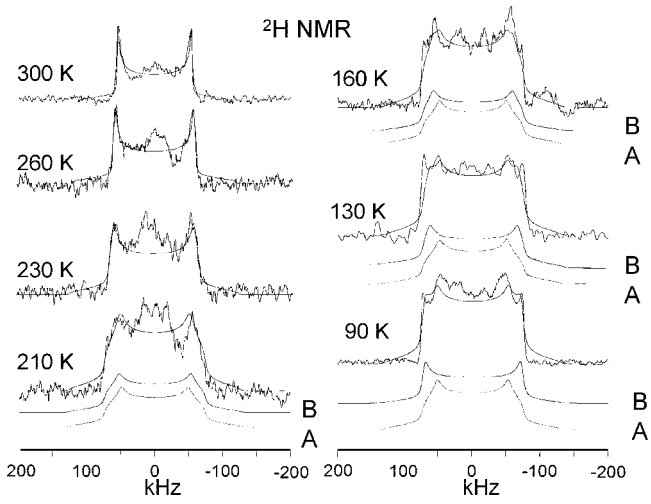

Figure 9. Superimposed experimental and calculated ^{2}H spectra of porphycene at selected temperatures. Two components for molecules A and B of equal intensities were assumed, using an intrinsic value of $q_{zz} = 150$ kHz and jumping angles of $\theta = 140°$ (see Scheme 1). Recycle delays were 1 s at 90 K, 2 s at 130 and 160 K, 3 s at 210 K, and 4 s at 230 K and above. For further information, see text.

SCHEME 1: (a) Changes of the ^{1}H−^{15}N Dipolar Interaction caused by H Transfer in a NHN Hydrogen Bond[a] and (b) Changes of the ^{2}H Quadrupole Interaction caused by D Transfer in a NDN hydrogen bond[b]

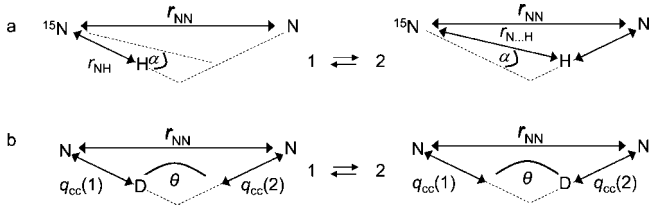

[a] r_{NH} and $r_{N\cdots H}$ represent the NH distance vectors before and after the transfer. α represents the jump angle. [b] $q_{cc}(1)$ and $q_{cc}(2)$ represent the quadrupole coupling constant in tautomers 1 and 2. θ represents the jump angle.

= 6.37 Hz. The calculated line components of A and B are included in Figure 9; their sum was superimposed on the calculated spectra.

It was assumed that deuteron sites exhibit the same intrinsic axially symmetric quadrupole coupling tensors $q_{cc}(1) = q_{cc}(2) = q_{cc} = 4q_{zz}/3$. We used in the calculation the thermodynamic parameters of the tautomerism of molecules A and B included in Table 2, and varied only the intrinsic jump angle θ and the value of q_{zz}, assumed to be independent of temperature. The best fit was obtained with $q_{zz} = 150$ kHz and jump angles of $\theta = 140°$. Above 225 K, we used the same parameters but only set the equilibrium constant to 1. The agreement between calculated and experimental line shapes is satisfactory. Moreover, the ^{2}H spectra confirm the phase change around 225 K.

In order to obtain information about the kinetics of the tautomerism we performed ^{2}H longitudinal relaxation experiments using the progressive saturation technique. All original data are assembled in the Supporting Information. As an example, Figure 10 shows the results of an experiment on porphycene-d_2 in phase II at 130 K.

The data of phase I were analyzed in terms of single exponential decays. In a first step, the same procedure was applied to the data of phase II. However, in a later refinement the different relaxation behavior of molecules A and B was taken into account, and the build-up curves were recalculated using the bi-exponential time dependence

$$I = I_{A\infty}[1 - \exp(-t/T_1^A)] + I_{B\infty}[1 - \exp(-t/T_1^B)] + I_o \quad (6)$$

Here, $I_{A\infty} = I_{B\infty}$ represent the equilibrium signal intensities of molecules A and B. I_o represents a signal contribution arising from imperfect pulses and an imperfect signal detection. A fixed ratio T_1^B/T_1^A was used determined as described in the next section. Thus, only three parameters, i.e. I_o, $I_{B\infty}$, and T_1^B were varied in order to describe the build-up curves. As example, Figure 11 displays the results obtained at 130 K. All results are included in the Supporting Information.

Relaxation Time Analysis. *^{15}N T_1.* The master equation for the spin−lattice relaxation rates of nuclei S caused by fluctuations of the heteronuclear dipolar interaction with spins I which exchange between two sites 1 and 2 has been derived previously.[40] For solids, this equation depends on the molecular

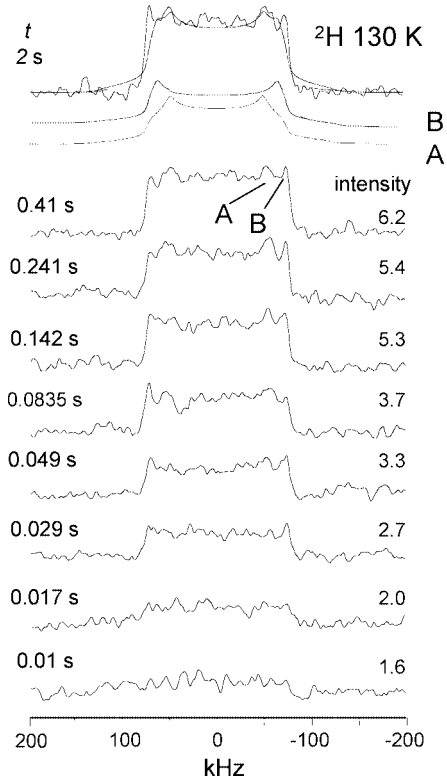

Figure 10. Measurement of the ^{2}H longitudinal relaxation times of a static powdered sample of porphycene-d_2 at 130 K and 46.03 MHz using the saturation recovery technique.

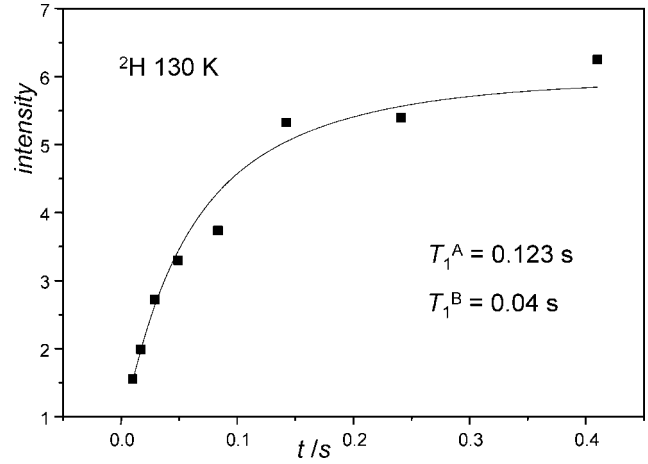

Figure 11. Analysis of the signal intensities of Figure 10 using a double exponential time dependence according to eq 6, by setting $T_{1B} = 0.35\ T_{1A}$. For further information see text.

orientation with respect to the external magnetic field. However, under MAS conditions, in the presence of a two-state tautomeric equilibrium between two forms 1 and 2, the T_1 values are given in very good approximation by the isotropic average.[19] For H transfer from and to ^{15}N the relaxation rate of the latter can then be expressed as

$$\frac{1}{T_{1N}} = \frac{1}{40}\gamma_N^2\gamma_H^2\hbar^2\left(\frac{\mu_o}{4\pi}\right)^2\frac{4K_{12}R}{(1+K_{12})^2}\left[\frac{\tau_c}{1+(\omega_H-\omega_N)^2\tau_c^2}+\frac{3\tau_c}{1+\omega_N^2\tau_c^2}+\frac{6\tau_c}{1+4(\omega_H+\omega_N)^2\tau_c^2}\right] \quad (7)$$

Here, $\mu_0 = 4\pi 10^{-7}$ T^2·m^3/J represents the permeability of the vacuum, γ_N and γ_H represent the gyromagnetic ratios of ^{15}N and of ^{1}H, ω_N and ω_H represent the corresponding Larmor frequencies and $\hbar = h/2\pi$, where h is Planck's constant. The inverse correlation time of the tautomerism is given by

$$\frac{1}{\tau_c} = k_{12}+k_{21} = k_{12}\left[\frac{1+K_{12}}{K_{12}}\right] = k_{21}[1+K_{12}] \quad (8)$$

where k_{12} and k_{21} are again the forward and backward rate constants of tautomerism. The dipolar interaction between the two spins gives rise to the geometric factor

$$R = r_{NH}^{-6}(1)+r_{NH}^{-6}(2)+r_{NH}^{-3}(1)r_{NH}^{-3}(2)(1-3\cos^2\alpha) \quad (9)$$

where $r_{NH}(1)$ and $r_{NH}(2)$ represent the NH distances in forms 1 and 2, and α represents the jump angle as defined in Scheme 1. In good approximation, one can assume that

$$R = r_1^{-6}+r_2^{-6}+r_1^{-3}r_2^{-3}(1-3\cos^2\alpha) \quad (10)$$

where r_1 represents the short NH distance and r_2 the long H···N distance of a given tautomer.

Equations 7−10 have been used to describe the longitudinal ^{15}N relaxation of porphycene.[6] The T_1 values (Table 3) are plotted in Figure 12a on a logarithmic scale as a function of the inverse temperature. The data points stem from the disordered phase I where the equilibrium constant of the tautomerism is $K_{12} = 1$. A broad T_1 minimum is observed around 270 K. A fit of the data to eq 7 and to a simple Arrhenius law gave the following parameters

$$E_a = 18 \text{ kJ mol}^{-1}, \quad A = 7\times10^{10} \text{ s}^{-1}, \quad R = 0.26 \text{ Å}^{-6} \quad (11)$$

In the next step, assuming that R is independent of temperature, we used eq 7 in order to convert the experimental ^{15}N T_1 values into rate constants k_{12} which are listed in Table 3. Their dependence on temperature and hence the dependence of the ^{15}N T_1 values on temperature leading to the solid line in Figure 12a was simulated using the Bell−Limbach tunneling model as described in the discussion.

^{2}H T_1. The longitudinal T_1 relaxation times of a deuteron with spin $I = 1$ experiencing a nondegenerate tautomerism between two states 1 and 2 are given by[41]

$$\frac{1}{T_{1I}} = \frac{3\pi^2}{10}\left(\frac{K_{12}}{(1+K_{12})^2}\right)C\left[\frac{\tau_c}{1+\omega_I^2\tau_c^2}+\frac{4\tau_c}{1+4\omega_I^2\tau_c^2}\right] \quad (12)$$

Here, the symbols have similar meanings as in eq 7. C in s^{-2} is a constant which depends on the quadrupole coupling constants q_{cc} in the two tautomeric states and on the jump angle θ between both tensors (Scheme 1). However, as noted before,[21] it is difficult to calculate C from the ^{2}H spectra. Therefore, in a similar way as the factor R in eq 7, C was treated as a parameter to be determined by the fit of the experimental data to eq 12.

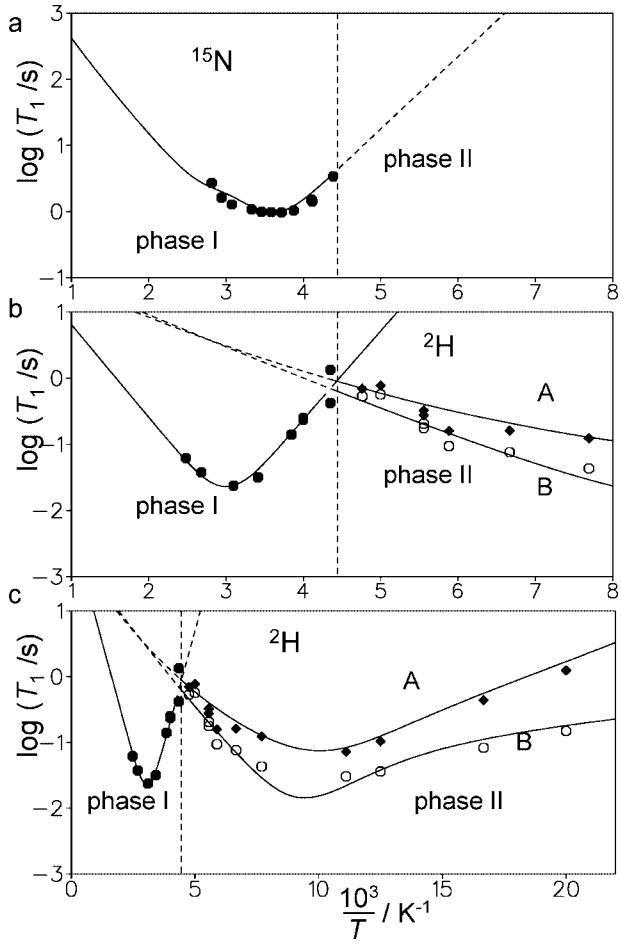

Figure 12. (a) Longitudinal ^{15}N relaxation times of porphycene obtained under CPMAS conditions at a frequency of 9.12 MHz as a function of the inverse temperature. Adapted from ref 1. (b and c) Longitudinal ^{2}H relaxation times of porphycene-d_2 obtained at 46.03 MHz. The solid lines were calculated as described in the text.

The results of the measurements are listed in Tables 4 and 5 and are depicted in Figure 12, parts b and c. For phase I we observe a clear minimum around 330 K. However, upon further lowering temperature to the phase transition temperature around 225 K a sudden change is observed, and in phase II the T_1 values decrease again, and go through a minimum around 90 K. Molecules A and B exhibit different values as discussed below.

The ^{2}H T_1 data of phase I were processed in a similar way as the ^{15}N data. Around the minimum, using eq 12 we obtained the following parameters which can describe the dependence of the ^{2}H T_1 values of phase I as a function of temperature

$$E_a = 25.4 \text{ kJ mol}^{-1}, \quad A = 4\times10^{12} \text{ s}^{-1}, \quad C = 1.2\times10^{10} \text{ s}^{-2} \quad (13)$$

Using the value of C, the ^{2}H T_1 values were converted into the rate constants of deuteron transfer in a similar way as described above for the ^{15}N data. We were astonished to find that around 260 K the rate constant of HH transfer was 2.0×10^7 s^{-1} and the one of DD transfer 1.5×10^7 s^{-1}. Both values coincide within the margin of error.

In the next step, we analyzed the data of phase II. The T_1 values averaged over both molecules (Table 5) indicate a T_1 minimum around 90 K. However, according to eq 12, both molecules A and B exhibit slightly different equilibrium constants K_{12} of tautomerism (Table 2) and hence different longitudinal relaxation times. As mentioned above, the signal-to-noise ratio did not allow us to obtain these values from the magnetization build-up curves directly. Therefore, we estimated $T_1{}^A$ and $T_1{}^B$ as follows.

It has been shown by Marcus,[42] that the following relation holds in good approximation between the rate and the equilibrium constants of proton transfer

$$k = \sqrt{k_{12}k_{21}}, \quad k_{12} = k\sqrt{K_{12}}, \quad k_{21} = \frac{k}{\sqrt{K_{12}}} \tag{14}$$

k represents the rate constant of the degenerate process where $K_{12} = 1$; i.e., it is the same for molecules A and B. It follows for the inverse correlation time that

$$\frac{1}{\tau} = k\left[\frac{1+K_{12}}{\sqrt{K_{12}}}\right] \tag{15}$$

After introducing labels for both molecules, we obtain by combination of eqs 12 and 15, the following ratio between the longitudinal relaxation times of both molecules

$$\frac{T_1{}^B}{T_1{}^A} = \left(\frac{\left(\frac{K_{12}^A}{K_{12}^B}\right)^{3/2}}{\left(\frac{1+K_{12}^A}{1+K_{12}^B}\right)^3}\right)\frac{\frac{1}{1+\frac{\omega_I^2}{k^2}\frac{K_{12}^A}{(1+K_{12}^A)^2}}+\frac{4}{1+\frac{4\omega_I^2}{k^2}\frac{K_{12}^A}{(1+K_{12}^A)^2}}}{\frac{1}{1+\frac{\omega_I^2}{k^2}\frac{K_{12}^B}{(1+K_{12}^B)^2}}+\frac{4}{1+\frac{4\omega_I^2}{k^2}\frac{K_{12}^B}{(1+K_{12}^B)^2}}} \tag{16}$$

If $\omega_I \ll k$, it follows that

$$\frac{T_1{}^B}{T_1{}^A} = \frac{K_{12}^A\sqrt{K_{12}^A}(1+K_{12}^B)^3}{K_{12}^B\sqrt{K_{12}^B}(1+K_{12}^A)^3} \tag{17}$$

and if $\omega_I \gg k$ that

$$\frac{T_1{}^B}{T_1{}^A} = \sqrt{\frac{K_{12}^A}{K_{12}^B}}\frac{1+K_{12}^B}{1+K_{12}^A} \tag{18}$$

Thus, the ratio $T_1{}^B/T_1{}^A$ depends on k only in the range of the T_1 minimum where $\omega_I \cong k$. Therefore, in order to determine this ratio, one needs a rough estimate of k. For that purpose, we assumed that k in the neighborhood of the T_1 minimum is given by a simple Arrhenius law, with the parameters

$$E_a = 9.2 \text{ kJ mol}^{-1}, \quad A = 4\times10^{12} \text{ s}^{-1} \tag{19}$$

The value of E_a was taken from the dependence of the average T_1 values in the temperature range between 210 and 130 K. The pre-exponential factor is the usual one for overbarrier proton transfer.[2] We obtained the values of $T_1{}^B/T_1{}^A$ listed in Table 5. We note again that changing the activation energy by about 1 kJ mol^{-1} did not affect the results significantly.

In the next step, each experimental saturation build-up curve was fitted to the double-exponential eq 6, keeping the ratio between $T_1{}^B$ and $T_1{}^A$ constant. In most cases, the fit was better than the single exponential fit as illustrated in the Supporting Information. The results are assembled in Table 5. The relaxation times of both molecules were then plotted in a logarithmic way as a function of the inverse temperature as depicted in Figure 12, parts b and c. Minima were observed for both $T_1{}^B$ and $T_1{}^A$. The values in the minima were reproduced with a single constant $C = 2.1 \times 10^{10}$ s^{-2}. In other words, the different relaxation times mainly arise from the different values of the equilibrium constants.

Finally, we converted the values of $T_1{}^B$ and $T_1{}^A$ into rate constants of tautomerism $k_{12}{}^B$ and $k_{12}{}^A$ using eq 12. The values obtained are included in Table 5. The Arrhenius curves obtained are depicted in Figure 13. The curves exhibit a non-Arrhenius behavior in the sense that the effective activation energies at low temperatures are smaller than at high temperatures. This result can be also directly derived from the different absolute slopes of the log T_1 vs $1/T$ curves of Figure 12. The solid lines in Figure 13 were simulated in terms of the Bell-Limbach tunneling model as described in the next section. Finally, the calculated rate constants were reconverted back into T_1 values, giving rise to the solid lines in the right part of Figures 12b and 12c which provide an excellent fit of the experimental data.

TABLE 4: ^{2}H T_1 Relaxation Times and Rate Constants $k_{12}{}^{DD}$ of Solid Porphycene-d_2 in Phase I[a]

sample	T/K	T_1/s	$k_{12}{}^{DD}$/s^{-1}
C	403	0.0617	1.32×10^9
C	373	0.0376	7.40×10^8
C	323	0.0237	1.70×10^8
C	293	0.0318	9.20×10^7
A	260	0.17	1.40×10^7
B	260	0.14	1.70×10^7
A	250	0.235	1.00×10^7
B	250	0.25	9.50×10^6
A	230	1.34	1.76×10^7
B	230	0.42	5.60×10^6

[a] Rate constants calculated using eq 12 and a value of $C = 1.2 \times 10^{10}$ s^{-2}.

TABLE 5: ^{2}H T_1 Relaxation Times and Rate Constants $k_{12}{}^{DD}$ of Solid Porphycene-d_2 in Phase II[a]

sample	T/K	T_1/s	$T_1{}^B/T_1{}^A$	$T_1{}^B$/s	$T_1{}^A$/s	$k_{12}{}^{DD}$ (B)/s^{-1}	$k_{12}{}^{DD}$ (A)/s^{-1}
A	210	0.6099	0.77	0.533	0.695	1.8×10^{10}	1.32×10^{10}
B	200	0.614	0.73	0.565	0.77	1.9×10^{10}	1.33×10^{10}
A	180	0.387	0.64	0.205	0.326	5.8×10^9	3.70×10^9
B	180	0.223	0.64	0.177	0.275	6.7×10^9	4.40×10^9
A	170	0.333	0.59	0.094	0.159	3.0×10^9	1.85×10^9
A	150	0.156	0.47	0.076	0.161	2.3×10^9	1.27×10^9
A	130	0.091	0.35	0.043	0.123	1.1×10^9	5.5×10^8
B	130	0.10	0.35	0.043	0.123	1.1×10^9	5.5×10^8
A	90	0.0474	0.42	0.0304	0.072	3.5×10^7	2×10^7
A	80	0.0672	0.35	0.036	0.1034	2.8×10^7	1.3×10^7
A	60	0.158	0.19	0.083	0.437	1.1×10^7	4×10^6
A	50	0.443	0.12	0.149	1.247	5.6×10^6	9×10^5

[a] Rate constants calculated using eq 12 and a value of $C = 2.0 \times 10^{10}$ s^{-2} for both molecules A and B. The values of $T_1{}^B/T_1{}^A$ were calculated as described in the text.

Discussion

Using a combination of ^{15}N and ^{2}H solid state NMR spectroscopy and longitudinal relaxation experiments we have studied the solid state tautomerism of porphycene (Figure 1), leading to the Arrhenius diagram of Figure 13. A very unusual behavior is observed. It was established that the solid is subject to a phase transition around 225 K. In the high-temperature

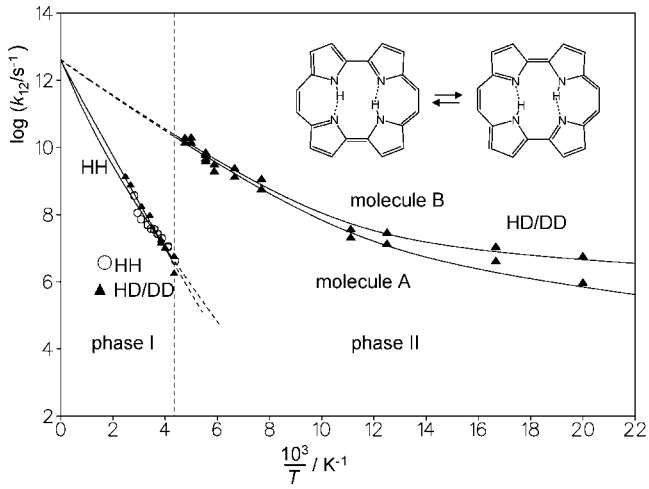

Figure 13. Arrhenius diagram of the double proton transfer of polycrystalline porphycene in phases I and II. The Arrhenius curves were calculated using the Bell−Limbach tunneling model as described in the text, using the parameters of Table 5.

phase I, the tautomerism is degenerated and the rate constants are much smaller than in the low-temperature phase II. Moreover, whereas in phase I no kinetic hydrogen/deuterium isotope effect is observed within the margin of error indicating an overbarrier reaction, a nonlinear Arrhenius curve of the deuteron motion is observed in two slightly different molecules A and B of phase II (Figure 1b) indicating a tunnel mechanism. In the following, we discuss these unexpected results as well as open questions in detail.

Phase Dependent Solid State Tautomerism of Porphycene: Structure and Thermodynamics. Let us first discuss in more detail the differences between the two phases. For phase I a single ^{15}N signal is observed[1,6] which implies a degenerate tautomerism, i.e., a "dynamic proton disorder". By contrast, for phase II four nitrogen signals are observed exhibiting temperature dependent line splittings. The temperature dependence arises from fast nondegenerate proton transfer processes. This is because intermolecular interactions lift the degeneracy of the tautomerism as has been well established previously.[31] This case would then correspond to a "dynamic proton order".

Clearly, in the low temperature phase there is a contribution of the tautomerism to the heat capacity of the solid, used to increase the mole fractions of the nondominant tautomers. Unfortunately, this contribution to the heat capacity may be small and difficult to measure. It is canceled in phase I, as the equilibrium constants of tautomerism are unity. Therefore, the proton order−disorder transition around 225 K may either correspond to a first order or a second order phase transition. A similar order−disorder phase transition was observed previously by ^{15}N CPMAS NMR for the case of 4-pyrazolecarboxylic acid, although the phase transition was extended over a larger temperature range.[43] Moreover, as hydrogen nuclei are difficult to be localized by X-ray crystallography it could not be observed using this method.

Previously,[6] we were not able to distinguish whether there is a single type of molecule in the unit cell of phase II containing four inequivalent nitrogen sites as is the case in the related TTAA molecule (Figure 5) or whether the unit cell contains two molecules A and B, where each molecule contains only two inequivalent nitrogen sites. As was illustrated in Figure 1, the first case would correspond to the presence of four tautomeric states 1 to 4, where the gas-phase degeneracy of the trans-tautomers 1 and 2 as well as of the cis-tautomers 3 and 4 is lifted by molecular interactions as found for TTAA.[31,32] In the second case, for each molecule only the two trans-states are observed, where the equilibrium constants are slightly different for molecules A and B. The ^{15}N magnetization transfer studies of Figures 6 and 7 clearly indicate that the second possibility is realized for porphycene. From the temperature-dependent splittings and the van't Hoff diagram of Figure 8 the thermodynamic parameters of the tautomerism of molecules A and B below 225 K were obtained, assembled in Table 2. The reaction entropies are very small, and the reaction enthalpies only 2.9 and 0.71 kJ mol^{-1}.

The order−disorder phase transition of solid porphycene was confirmed by the analysis of the ^{2}H spectra of static powdered samples of porphycene-d_2 (Figure 9). For phase I only a single deuteron type is observed, which is subject to a fast tautomerism, whereas two different kinds of deuterons are observed for phase II. The spectra in the latter phase could be simulated in terms of a fast exchange between two unequally populated sites using the thermodynamic parameters of Table 2, by adapting the quadrupole coupling constant and the jump angle $\theta = 140°$ defined in Figure 9. This means that the hydrogen bonds in porphycene are not linear but slightly bent. In fact, quantum chemical calculations (B3LYP, 6-31G(d,p)) predict an angle of about 153°.[12]

Phase Dependent Solid State Tautomerism of Porphycene: Longitudinal Relaxation and Proton and Deuteron Dynamics. A further confirmation of the phase transition was provided by longitudinal ^{2}H T_1 relaxation experiments of porphycene-d_2 performed at 46.03 MHz. As illustrated in Figure 12, parts b and c, ^{2}H T_1 minima were obtained for both phases, i.e., 330 K for phase I and 90 K for phase II. At the phase transition temperature, the temperature dependence of T_1 suddenly changes. It is difficult to say in view of the large margin of error whether the ^{2}H T_1 relaxation times change suddenly at the phase transition or whether they just go through a maximum. For a first order phase transition one would expect a sudden jump.

The interpretation of the deuteron relaxation behavior in phase II is straightforward. The slope of the log T_1 vs $1/T$ curve in phase II (Figure 12c) is much smaller below than above the minimum. This is a typical sign of deuteron tunneling.[2,22−25] This establishes clearly that the dynamic process causing the change of the deuteron quadrupole coupling tensor and hence deuteron relaxation in phase II is the deuteron transfer.

By contrast, the log T_1 vs $1/T$ curve for phase I is symmetric with respect to the minimum indicating an overbarrier reaction. Previously, we had observed for phase I a ^{15}N T_1 minimum of porphycene-h_2 at 9.12 MHz (Figure 12a) which was discussed in terms of a dipolar relaxation mechanism, where the proton tautomerism modulates the ^{1}H−^{15}N dipolar interaction. However, the activation energy of about 18 kJ mol^{-1} (eq 11) seemed to be too large as compared to related proton transfer systems.[2]

At first sight, it is tempting to associate the high-temperature process to a "horizontal" tautomerism as was illustrated in Figure 3. However, this process is very slow in the liquid at room temperature, i.e. slower than the millisecond time scale. Hence, it can not cause the observed relaxation patterns of solid porphycene, and we will not discuss this process any longer.

On the other hand, we checked again whether the observed ^{15}N and ^{2}H relaxation behavior in phase I may be explained not by the "vertical" tautomerism but by other molecular motions, for example, rotations of the whole porphycene molecule. We remind that in the case of porphyrin a combined nondegenerate proton transfer coupled to a 180° rotation of the whole molecule around the z-axis perpendicular to the molecular

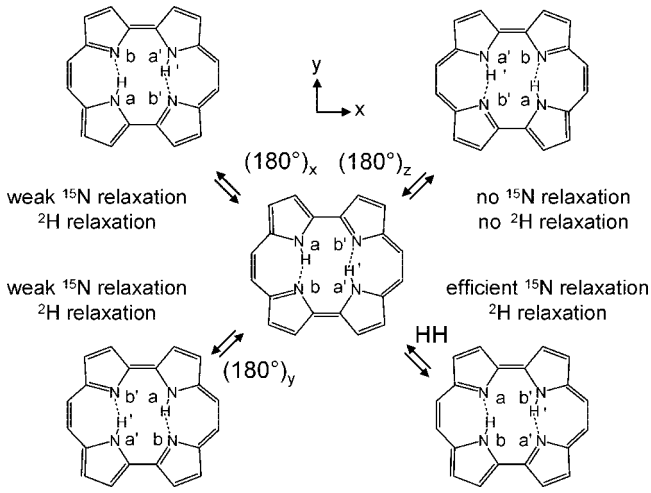

Figure 14. Influence of molecular 180° rotations and of the tautomerism of porphycene on various longitudinal relaxation mechanisms.

plane had been postulated[44] to explain the ^{15}N solid state NMR spectra;[1] however, it was later shown that the observed kinetic HH/HD/DD isotope effects of the solid state porphyrin tautomerism imply a degenerate double proton transfer.[7a]

In order to facilitate the discussion we compare in Figure 14 the effects of molecular rotations around the three molecular axes of porphycene in phase I and of the proton respective deuteron tautomerism on the dipolar $^1H-^{15}N$ interaction and of the quadrupole ^2H interaction. For a $(180°)_z$ rotation around the molecular z-axis the factor R in eq 10 and the factor C in eq 12 vanish. Thus, this rotation is not a source of relaxation. $(180°)_x$ rotations, $(180°)_y$ rotations, and deuteron transfer modulate the ^2H quadrupole interaction in the same way and are a source of relaxation if C is nonzero, i.e., if the deuteron jump angle θ (Figure 9) is different from 180°. As the ^2H quadrupole interaction is much larger than the dipolar $^1H-^{15}N$ interaction, the latter contributes to relaxation, i.e., R is large only if the NH distance is modulated; a small reorientation of the NH-vector in space is not sufficient.

The analysis of the factor $R = 0.26$ Å^{-6} in eq 11 presented previously[6] showed that the ^{15}N T_1 value of the minimum is consistent with a variation of the $^{15}N-^1H$ distance from about 1.1 to 1.6 Å. These values were recently confirmed by first principle calculations.[12] In other words, the ^{15}N relaxation in phase I (Figure 12a) is not caused by molecular rotations but by the proton tautomerism.

Further insights come from a discussion of the rate constants (Tables 3 and 4, Figure 13) derived from the ^{15}N T_1 and ^2H T_1 data as described in the preceding section. We already pointed out that the rate constants of the processes derived from the relaxation of the two kinds of nuclei coincide within the margin of error. This means that the two processes observed by ^{15}N and ^2H relaxometry are both hydron transfers which do not exhibit substantial kinetic hydrogen/deuterium isotope effects. The margin of error is compatible with values up to 2; moreover, we can not exclude also the presence of inverse isotope effects where the DD transfer is faster than the HH transfer. The small isotope effects can also explain why we were not able to detect an influence of the deuteron fraction on the ^2H T_1 values: if the rate constants of the HD and the DD transfer are the same, the ^2H T_1 values of porphycene-*hd* and of porphycene-d_2 will also be the same.

Finally, molecular rotations such as those depicted in Figure 14 will exhibit large activation energies of probably more than 40 kJ mol^{-1}, i.e. much larger than found here for the tautomerism of phase I. Also a mechanism is unlikely, which has been established for solid tropolone, exhibiting a barrier of more than 80 kJ mol^{-1}, where in a given molecular site only a single tautomer is populated, but where molecular jumps between adjacent sites are coupled to proton jumps.[45]

Our observation that the constant C in eq 12, which determines the T_1 values in the minima, is 1.2×10^{10} s^{-2} for phase I and 2.1×10^{10} s^{-2} indicates a smaller jump angle θ in phase II, i.e., a more nonlinear hydrogen bond.

Arrhenius Curves of the Porphycene Tautomerism. Let us now first discuss the resulting Arrhenius diagram of the porphycene tautomerism depicted in Figure 13. For phase I, the tautomerism was degenerate, i.e. the forward and backward rate constants are the same. For phase II, we plotted the forward rate constants k_{12} of the deuteron transfer, where 1 corresponds to the dominant state and 2 to the nondominant state. As the asymmetry is larger for molecule A according to Table 2, the forward rate constants of molecule A are smaller than those of molecule B. Nevertheless, both Arrhenius curves of phase II exhibit a concave curvature. The solid lines were calculated using the Bell−Limbach tunnel model described previously,[2] using the parameters listed in Table 6. We note that the parameter set indicated may not be unique, and subject to changes if more data could be obtained. Moreover, the Bell−Limbach model is only preliminary and the application of first-principle methods is desirable in the future.

A minimum energy E_m for tunneling to occur of about 0.6 and 1.9 kJ mol^{-1} was found for molecules A and B; the difference arises from the different reaction enthalpies of the two molecules. At higher temperatures, the slope is determined by the sum $E_m + E_d$, where the barrier height E_d was only 9.6 and 8.8 kJ mol^{-1} for the DD transfer in molecules A and B, respectively. The tunneling distances $2a$ were 0.52 Å and 0.56 Å, and the usual frequency factor A was $10^{12.6}$ s^{-1}. The tunneling mass of the two deuterons was 4, and an additional tunneling mass Δm arising from heavy atom tunneling during the DD transfer was 1.5. Unfortunately, we were not able to determine the kinetic isotope effects for phase II.

For phase I very different parameters are obtained. For the DD reaction only an effective barrier $E_m + E_d$ of 27.2 kJ mol^{-1} was obtained, keeping the pre-exponential factor to a value of $10^{12.6}$ s^{-1}. Tunnel parameters for the HH reaction are included in Table 6, as they gave a slightly better fit of the rate constants of this process as compared to a simple Arrhenius law.

In Figure 15 we compare the kinetic data of the solid state tautomerism of porphycene obtained here with related kinetic data of other processes whose tunnel parameters are also included in Table 6. We note that the Arrhenius curve of the DD reaction in phase II and hence the tunnel parameters are very similar to the Arrhenius curve for the single D transfer in solid amorphous *N*,*N*′-diphenyl-6-aminofulvene-1-aldimine[21](PALDIM). This molecule exhibits a seven-membered H-chelate structure with NHN hydrogen bond geometries similar to those of porphycene.[11] For PALDIM, it was found that the tautomerism is much slower in the crystalline state as compared to an amorphous phase. However, there was no distinct transition between the two phases at a given temperature, in contrast to porphycene. Therefore, if such a transition had existed for PALDIM, a drastic change of the H transfer kinetics would have been observed too. The good agreement between the D transfer rates in amorphous PALDIM and the DD transfer rates in porphycene make it plausible that the HH transfer in phase II of porphycene is as fast as the H transfer in PALDIM, i.e. that

TABLE 6: Barrier Height E_d and Minimum Energy for Tunneling E_m in kJ mol^{-1}, Barrier Width $2a$ in Å, Frequency Factor A in s^{-1}, and Tunneling Masses $m_{eff}^L = m^L + \Delta m$ (L = H, D)

	k(298 K)/s^{-1}	E_d	E_m	$E_d + E_m$	log A/s^{-1}	$2a$/Å	m^L	Δm
porphyrin HH	16000	28.7	22.7	51.4	12.6	0.68	1	1.5
porphyrin HD/DD	1400	32.6	22.7	55.3	12.6	0.68	2	1.5
porphyrin anion H	10^5	34.3	10.0	44.3	12.6	0.78	1	1.5
porphyrin anion D	6000	40.8	10.0	50.8	12.6	0.78	2	1.5
PALDIM crystalline H	$\approx 3.7 \times 10^{10}$	10.2	2.1	12.3	12.6	0.66	1	1.0
PALDIM crystalline D	$\approx 4.1 \times 10^9$	15.4	2.1	17.5	12.6	0.66	2	1.0
PALDIM amorphous H	$\approx 2.2 \times 10^{11}$	5.9	2.1	8.0	12.6	0.40	1	1.5
PALDIM amorphous D	$\approx 5.8 \times 10^{10}$	9.0	2.1	11.1	12.6	0.40	2	1.5
porphycene HH phase I	$\approx 5.8 \times 10^7$	15.1	20.1	35.2	12.6	0.20	2	0
porphycene DD phase I	$\approx 7.5 \times 10^7$			27.2	12.6			
porphycene DD phase II A	$\approx 6.3 \times 10^{10}$	8.8	1.9	10.7	12.6	0.52	2	1.5
porphycene DD phase II B	$\approx 7.4 \times 10^{10}$	9.6	0.63	10.3	12.6	0.56	2	1.5

there is a large kinetic HH/DD isotope effect of the tautomerism of porphycene in phase II, by contrast to phase I.

Another comparison is interesting. In Figure 15 are included kinetic data obtained by Waluk et al.[4,10] for the tautomerism of electronically excited porphycene-h_2 embedded in polyvinylbutyral. The data represent averages of the forward and backward rate constants k_{12} and k_{21}, as well as averages over a distribution of local environments exhibiting different equilibrium constants of tautomerism, as found previously for TTAA (Figure 5) in polystyrene.[32] We note that the rate constants of the H transfer of porphycene in the electronically excited-state are similar to those of the DD tautomerism in the electronic ground-state of phase II of porphycene.

Temperature Dependent Reaction Energy Profile of the Tautomerism of Porphycene. The question then arises which conclusions might be drawn concerning the mechanism of the porphycene tautomerism. The main conclusion is that there is a strong dependence on the environment which may make it difficult to compare condensed matter kinetics of porphycene with those obtained for the gas phase. This comparison was possible for porphyrin[1] which exhibits a much higher barrier of the tautomerism than porphycene. Thus, as is also demonstrated by the case of PALDIM, the dependence of the H transfer kinetics on the environment increases with a reduction of the barrier, i.e. with a strengthening of the hydrogen bond in which the transfer takes place.

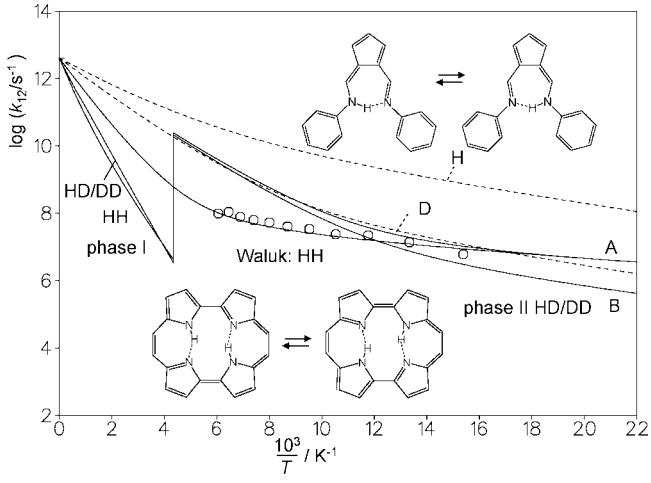

Figure 15. Comparison of the Arrhenius curves of related solid state hydrogen transfer reactions. Solid lines: HH and DD transfer of porphycene in phase I, of DD transfer in porphycene molecule B in phase II, of HH transfer in electronically excited porphycene, embedded in polyvinylbutyral according to Waluk et al.[4,10] Dashed lines: H and D transfer in amorphous solid N,N′-diphenyl-6-aminofulvene-1-aldimine according to ref 21 (upper dashed curves).

The similarity of porphycene in phase II with amorphous PALDIM could indicate a stepwise proton transfer in phase II of porphycene as illustrated in Figure 16a. For the condensed phase it is reasonable to assume that intermolecular interactions do not only lift the degeneracy between tautomers 1 and 2 as illustrated schematically in Figure 16a, but also between cis-tautomers 3 and 4. Thus, one of them (e.g., 3) might be lower in energy as compared to the other (e.g., 4) what could give rise to a very efficient and fast stepwise H transfer pathway.

In order to discuss this effect further let us consider the influence of an electric field which could be produced by a crystalline environment on the energetics of the porphycene tautomerism. The molecule shall be oriented as shown in Figure 16. Let us assume the presence of an electric field in the y-direction. In dipole approximation, this field does not change the relative energies of the trans tautomers 1 and 2. By contrast, the cis tautomer 3 exhibits a dipole moment of about 1.3 Debye (B3LYP, 6-31+G(d,p)) along the y-direction, and the cis tautomer 4 along the $-y$ direction. In other words, in a field directed along the y-axis one cis tautomer 3 will be stabilized in energy and cis tautomer 4 destabilized as illustrated schematically in Figure 16a.

So far we have tacitly assumed that the solid state environment is static. Upon increasing temperature, fluctuations will become more important and the discussed effect might become averaged out, that is, the H-atoms experience some effective potential due to the fluctuating environment. If this is indeed the case, the present observation of two distinct phases suggests that the transition does not occur gradually but abruptly around a temperature of 225 K. Indeed in phase I experimental evidence for a degenerate tautomerism would be compatible with the energy pathway illustrated schematically in Figure 16b. Here, the difference between the energies of the cis-intermediate states 3 and 4 might have disappeared due to environmental fluctuations. This could also lead to an energy plateau as has been postulated for other double proton transfer reactions.[46,47]

In Figure 16c and 16d the reaction energy profiles of a concerted double proton transfer in the two phases are depicted schematically. The transition state 5‡ does not have a permanent dipole moment. Therefore, it is unlikely that electric fields exert a strong influence on the reaction profile, which is again slightly asymmetric in phase II but symmetric in phase I. In phase II, the concerted transfer mechanism may not constitute a competing pathway as compared to the stepwise transfer. However, it could be that the concerted transfer is dominant in phase I, as a consequence of the shorter path. Usually concerted HH transfers exhibit substantial kinetic HH/DD isotope effects (KIE)[2,48] which seem to be in contrast to our findings in Figure 13 for phase I. Small isotope effects are expected for a plateau

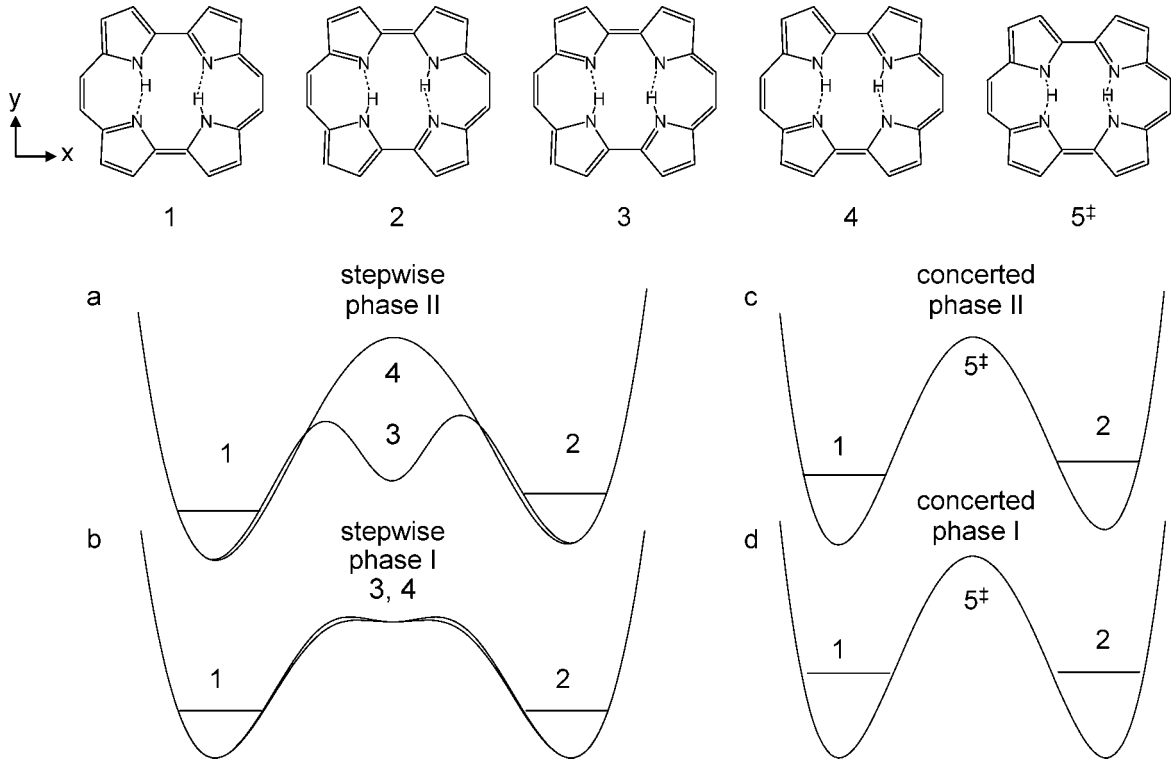

Figure 16. Possible minimum energy pathways (schematically) for the double proton transfer in solid porphycene. (a) Stepwise transfer in phase II in the presence of intermolecular interactions, which lift the degeneracy between the two trans-intermediates, and which strongly increase the energy of the cis-intermediate 3 but decrease the energy of 4. The transfer then dominantly proceeds via 4. (b) Profiles of the stepwise transfer in phase I. The energy difference between 1 and 2 as well as between 3 and 4 has disappeared. (c and d) Corresponding profiles of the concerted transfer in phases II and I. For further information see text.

reaction[46b] (Figure 16b) or for a concerted transfer in a state where both hydrogen bonds are strongly compressed.[49] Focusing on the latter aspect, there are two reasons for the occurrence of kinetic isotope effects. On one hand, fractionation factor theory in combination with transition state theory constitutes the classical theory of kinetic H/D isotope effects of proton transfer reactions as shown be Bigeleisen and Wolfsberg.[50] Wolfsberg et al.[51] have developed the theory of anharmonic corrections to isotope effects. On the other hand, tunneling strongly influences the KIE as proposed by Bell.[2,52] If prior to compression no tunneling occurs, and if the barrier in the compressed state is small, then the KIE will not be strongly affected by tunneling. On the other hand, zero-point energy changes during compression might be small.[53] This effect could arise from an increase of NH-bending and of a decrease of NH-stretching frequencies between the initial and the transition state.

In this discussion, one should however keep in mind that the notion of a stepwise and a concerted transfer represents limiting cases of a more complex mechanism. For example, it has been proposed previously[2,21,54] that the difference between the concerted and stepwise transfer disappears when hydrogen bond compression precedes the H transfer. For porphycenes, it has been shown recently that compression of one NHN-bond leads to a compression of the other.[11,12] Thus, a possible mechanism for phase I could be as follows: in a first step of the reaction pathway both bonds may be compressed and both hydrogen atoms shifted toward the hydrogen bond center without much tunneling and zero-point energy changes. From this state a more or less concerted motion of both protons could occur.

Conclusions

Using a combination of ^{15}N and ^{2}H solid state NMR spectroscopy and relaxometry we have derived the following very unusual results concerning the solid state tautomerism of porphycene. Above 225 K, in a high-temperature phase (phase I) the HH transfer is degenerate and takes place on the microsecond time scale, exhibiting a barrier of about 30 kJ mol^{-1} but only small kinetic HH/DD isotope effects. By contrast, at the phase transition to the low-temperature phase (phase II) the rate constants of the DD tautomerism are increased by 4 orders of magnitude, exhibiting a barrier of only 10 kJ mol^{-1}; moreover, the degeneracy of the tautomerism is lifted. Measurements down to 50 K revealed strong tunneling contributions of the DD tautomerism. This very unusual behavior is discussed in terms of electric field effects which stabilize one of the cis-tautomers in phase II, but by a more or less concerted transfer in phase I.

Previously we had found that the barriers of the tautomerism of the structural isomer porphyrin and of its anion[2,7] are much larger, but effects of the environments were absent: the reactions were as fast in solution as well as in the solid state. On the other hand, for a single H transfer in a seven-membered H-chelate (Figure 15) we had also observed very large differences in the dynamics of proton transfer in an amorphous and in a crystalline form. Thus, we conclude that the smaller the barriers are, the more the reaction pathways are influenced by intermolecular interactions. This constitutes a challenge for theoretical studies that need to include the environment in order to reproduce experimental kinetic data.

Acknowledgment. The financial support of the Deutsche Forschungsgemeinschaft, Bonn-Bad Godesberg and the Fonds der Chemischen Industrie, Frankfurt, is gratefully acknowledged.

Supporting Information Available: Figures S1−S14, showing ^{2}H NMR T_1 measurements and data analysis of static samples of solid porphycene-d_2 as a function of temperature.

This material is available free of charge via the Internet at http://pubs.acs.org.

References and Notes

(1) Wehrle, B.; Limbach, H. H.; Köcher, M.; Ermer, O.; Vogel, E. *Angew. Chem., Int. Ed.* **1987**, *26*, 934–936.

(2) Limbach, H. H. Single and multiple hydrogen/deuterium transfer reactions in liquids and solids. In *Hydrogen Transfer Reactions*. Hynes, J. T., Klinman, J., Limbach,H. H., Schowen, R. L., Eds.; Wiley-VCH: Weinheim, Germany, 2007; *Vols. 1 & 2*, Chapter 6, pp 135−221, and references cited therein.

(3) Limbach, H. H.; Lopez, J. M.; Kohen, A. *Phil. Trans. B (London).* **2006**, *361*, 1399–1415.

(4) Waluk, J. Tautomerization in Porphycene. In *Hydrogen Transfer Reactions*; Hynes, J. T., Klinman, J., Limbach, H. H., Schowen, R. L., Eds.; Wiley-VCH: Weinheim, Germany 2007; *Vols. 1 & 2*, Chapter 8, pp 245−272.

(5) Vogel, E.; Köcher, M.; Schmickler, H.; Lex, J. *Angew. Chem., Int. Ed.* **1986**, *25*, 257–259.

(6) Langer, U.; Hoelger, Ch.; Wehrle, B.; Latanowicz, L.; Vogel, E.; Limbach, H. H. *J. Phys. Org. Chem.* **2000**, *13*, 23–34.

(7) (a) Braun, J.; Schlabach, M.; Wehrle, B.; Köcher, M.; Vogel, E.; Limbach, H. H. *J. Am. Chem. Soc.* **1994**, *116*, 6593–6604. (b) Braun, J.; Limbach, H. H.; Williams, P.; Morimoto, H.; Wemmer, D. *J. Am. Chem. Soc.* **1996**, *118*, 7231–7232. (c) Schlabach, M.; Wehrle, B.; Rumpel, H.; Braun, J.; Scherer, G.; Limbach, H. H. *Ber. Bunsenges. Phys. Chem.* **1992**, *96*, 821–833. (d) Braun, J.; Schwesinger, R.; Williams, P. G.; Morimoto, H.; Wemmer, D. E.; Limbach, H. H. *J. Am. Chem. Soc.* **1996**, *118*, 11101–11110. (e) Wehrle, B.; Limbach, H. H. *Chem. Phys.* **1989**, *136*, 223–247. (f) Schlabach, M.; Wehrle, B.; Limbach, H. H.; Bunnenberg, E.; Knierzinger, A.; Shu, A.; Tolf, B. R.; Djerassi, C. *J. Am. Chem. Soc.* **1986**, *108*, 3856–3858. (g) Schlabach, M.; Limbach, H. H.; Bunnenberg, E.; Shu, A.; Tolf, B. R.; Djerassi, C. *J. Am. Chem. Soc.* **1993**, *115*, 4554–4565.

(8) (a) Malsch, T.; Hohlneicher, G. *J. Phys. Chem. A* **1997**, *101*, 8409–8416. (b) Malsch, T.; Roeb, M.; Karuth, V.; Hohlneicher, G. *Chem. Phys.* **1998**, *227*, 331–348.

(9) (a) Sepioł, J.; Stepanenko, Y.; Vdovin, A.; Mordzinski, A.; Vogel, E.; Waluk, J. *Chem. Phys. Lett.* **1998**, *296*, 549–556. (b) Galievsky, V.; Starukhin, A.; Vogel, E.; Waluk, J. *J. Phys. Chem. A* **1998**, *102*, 4966–4971. (c) Starukhin, A.; Vogel, E.; Waluk, J. *J. Phys. Chem. A* **1998**, *102*, 9999–10006. (d) Gil, M.; Jasny, J.; Vogel, E.; Waluk, J. *Chem. Phys. Lett.* **2000**, *323*, 534–541. (e) Dobkowski, J.; Galievsky, V.; Starukhin, A.; Vogel, E.; Waluk, J. *J. Phys. Chem. A* **1998**, *102*, 4966–4971. (f) Waluk, J. *Acc. Chem. Res.* **2006**, *39*, 945–952. (g) Vdovin, A.; Sepioł, J.; Urbańska, N.; Pietraszkiewicz, M.; Mordziñski, A.; Waluk, J. *J. Am. Chem. Soc.* **2006**, *126*, 2577–2586.

(10) Gil, M.; Waluk, J. *J. Am. Chem. Soc.* **2007**, *129*, 1335–1341.

(11) Pietrzak, M.; Shibl, M. F.; Bröring, M.; Kühn, O.; Limbach, H. H. *J. Am. Chem. Soc.* **2007**, *129*, 296–304.

(12) Shibl, M. F.; Pietrzak, M.; Limbach, H. H.; Kühn, O. *ChemPhysChem* **2007**, *8*, 315–321.

(13) Kozlowski, P. M.; Zgierski, M. Z.; Baker, J. *J. Chem. Phys.* **1998**, *109*, 5905–5913.

(14) Cybulski, H.; Pecul, M.; Helgaker, T.; Jaszunski, M. *J. Phys. Chem. A* **2005**, *109*, 4162–4171.

(15) Walewsky, L; Krachtus, D.; Fischer, S.; Smith, J. C.; Bala, P.; Lesyng, B *Int. J. Quantum Chem.* **2006**, *106*, 636–640.

(16) Smedarchina, Z.; Shibl, M. F.; Kühn, O.; Fernández-Ramos, A. *Chem. Phys. Lett.* **2007**, *436*, 314–321.

(17) (a) Kwon, O. H.; Zewail, A. H. *Proc. Natl. Acad. Sci. U.S.A.* **2007**, *104*, 8703–8708. (b) Sekiya, H.; Sakota, K. *J. Photochem. Photobiol. C* **2008**, *9*, 81–91.

(18) (a) Limbach, H. H.; Manz, J. *Ber. Bunsen-Ges. Phys. Chem.* **1998**, *102*, 289–291. (b) Schowen, K. B.; Limbach, H. H.; Denisov, G. S.; Schowen, R. L. *Biochem. Biophys. Acta* **2000**, *1458*, 43–62.

(19) Hoelger, C. G.; Wehrle, B.; Benedict, H.; Limbach, H. H. *J. Phys. Chem.* **1994**, *98*, 843–851.

(20) Langer, U.; Latanowicz, L.; Hoelger, Ch.; Buntkowsky, G.; Vieth, H. M.; Limbach, H. H. *Phys. Chem. Chem. Phys.* **2001**, *3*, 1446–1458.

(21) Lopez del Amo, J. M.; Langer, U.; Torres, V.; Buntkowsky, G.; Vieth, H. M.; Pérez-Torralba, M.; Sanz, D.; Claramunt, R. M.; Elguero, J.; Limbach, H. H. *J. Am. Chem. Soc.* **2008**, *130*, 8620–8632.

(22) Xue, Q. A.; Horsewill, A. J.; Johnson, M. R.; Trommsdorff, H. P. *J. Chem. Phys.* **2004**, *120*, 11107–11119.

(23) Brougham, D. F.; Caciuffo, R.; Horsewill, A. J. *Nature* **1999**, *397*, 241–243.

(24) Takeda, S.; Inabe, T.; Benedict, C.; Langer, U.; Limbach, H. H. *Ber. Bunsen-Ges. Phys. Chem.* **1998**, *102*, 1358–1369.

(25) (a) Horsewill, A. J.; Heideman, A.; Hayashi, S. Z. *Phys. B.* **1993**, *90*, 319–324. (b) Meier, B. H.; Graf, F.; Ernst, R. R. *J. Chem. Phys.* **1982**, *76*, 767–774. (c) Stöckli, A.; Meier, B. H.; Kreis, R.; Meyer, R.; Ernst, R. R. *J. Chem. Phys.* **1990**, *93*, 1502–1520. (d) Heuer, A.; Haeberlen, U. *J. Chem. Phys.* **1991**, *95*, 4201–4214.

(26) Hayashi, S.; Hayamizu, K. *Bull. Chem. Soc. Jpn.* **1991**, *64*, 688–690.

(27) Du Bois Murphy, P. *J. Magn. Reson.* **1986**, *70*, 307–312.

(28) Torchia, D. *J. Magn. Reson.* **1978**, *30*, 613–616.

(29) Kendrick, R. D.; Friedrich, S.; Wehrle, B.; Limbach, H. H.; Yannoni, C. S. *J. Magn. Reson.* **1985**, *65*, 159–161.

(30) Rumpel, H.; Limbach, H. H. *J. Am. Chem. Soc.* **1989**, *111*, 5429–5441.

(31) Schlabach, M.; Rumpel, H.; Limbach, H. H. *Angew. Chem., Int. Ed. Engl.* **1989**, *28*, 76–79.

(32) Limbach, H. H.; Wehrle, B.; Schlabach, M.; Kendrick, R.; Yannoni, C. S. *J. Magn. Reson.* **1988**, *77*, 84–100.

(33) (a) Limbach, H. H.; Wehrle, B.; Zimmermann, H.; Kendrick, R.; Yannoni, C. S. *Angew. Chem.* **1987**, *99*, 241–243; *Angew. Chem. Int. Ed. Engl.* **1987**, *26*, 247−248. (b) Limbach, H. H.; Wehrle, B.; Zimmermann, H.; Kendrick, R.; Yannoni, C. S. *J. Am. Chem. Soc.* **1987**, *109*, 929–930.

(34) Wehrle, B.; Zimmermann, H.; Limbach, H. H. *J. Am. Chem. Soc.* **1988**, *110*, 7014–7024.

(35) (a) Wehrle, B.; Aguilar-Parrilla, F.; Limbach, H. H. *J. Magn. Reson.* **1990**, *87*, 584–591. (b) Aguilar-Parrilla, F.; Wehrle, B.; Bräunling, H.; Limbach, H. H. *J. Magn. Reson.* **1990**, *87*, 592–597.

(36) Morris, G. A.; Freeman, R. *J. Magn. Reson.* **1978**, *29*, 433–462.

(37) Auchus, R. J.; Covey, D. F.; Bork, V.; Schaefer, J. *J. Biol. Chem.* **1988**, *263*, 11640–11645.

(38) Goedken, V. L.; Pluth, J. J.; Peng Shie-Ming, S. M.; Bursten, B. *J. Am. Chem. Soc.* **1976**, *98*, 8014–8021.

(39) Macho, V.; Brombacher, L.; Spiess, H. W. *Appl. Magn. Reson.* **2001**, *20*, 405–432.

(40) Andrew, E. R.; Latanowicz, L. *J. Magn. Reson.* **1986**, *68*, 232–239.

(41) Medycki, W. R.; Reynhardt, E. C.; Latanowicz, L. *Mol. Phys.* **1998**, *93*, 323–328.

(42) Marcus, R. A. *Faraday Discuss. Chem. Soc.* **1982**, *74*, 7–15.

(43) Foces-Foces, C.; Echevarría, A.; Jagerovic, N.; Alkorta, I.; Elguero, J.; Langer, U.; Klein, O.; Minguet-Bonvehí, M.; Limbach, H. H. *J. Am. Chem. Soc.* **2001**, *123*, 7898–7906.

(44) Frydman, L.; Olivieri, A. C.; Diaz, L. E.; Frydman, B.; Kustanovich, I.; Vega, S. *J. Am. Chem. Soc.* **1989**, *111*, 7001–7002.

(45) Titman, J. J.; Luz, Z.; Spiess, H. W. *J. Am. Chem. Soc.* **1992**, *114*, 3756–3765.

(46) (a) Schweiger, S.; Rauhut, G. *J. Phys. Chem. A* **2003**, *107*, 9668–9678. (b) Schweiger, S.; Hartke, B.; Rauhut, G. *Phys. Chem. Chem. Phys.* **2004**, *6*, 3341–3349.

(47) Limbach, H. H.; Männle, F.; Denisov, G. S.; Detering, C. *Chem. Phys.* **2005**, *319*, 69–92.

(48) Lopez, J. M.; Männle, F.; Wawer, I.; Buntkowsky, G.; Limbach, H. H. *Phys. Chem. Chem. Phys.* **2007**, *9*, 4498–4513.

(49) Klein, O.; Aguilar-Parrilla, F.; Lopez, J. M.; Jagerovic, N.; Elguero, J.; Limbach, H. H. *J. Am. Chem. Soc.* **2004**, *126*, 11718–11732.

(50) Bigeleisen, J.; Wolfsberg, M. *Adv. Chem. Phys.* **1958**, *1*, 15–76.

(51) Wolfsberg, M. *Acc. Chem. Res.* **1972**, *5*, 225–233.

(52) Bell, R. P. *The Tunnel Effect*; Chapman and Hall: London, 1980.

(53) Smirnov, S. N.; Benedict, H.; Golubev, N. S.; Denisov, G. S.; Kreevoy, M. M.; Schowen, R. L.; Limbach, H. H. *Can. J. Chem.* **1999**, *77*, 943–949.

(54) Meschede, L.; Limbach, H. H. *J. Phys. Chem.* **1991**, *95*, 10267–10280.

JP8079414